Observation of finite-size-induced emission decay rates in self-assembled photonic crystals

Megha Khokhar, Priya,* and Rajesh V. Nair†
Laboratory for Nano-scale Optics and Meta-materials (LaNOM) Department of Physics, Indian Institute of Technology Ropar, Rupnagar, Punjab 140001, India

(Received 13 February 2020; accepted 1 June 2020; published 6 July 2020)

We study the extent of spontaneous emission inhibition in self-assembled photonic crystals where the light path is routinely affected by unavoidable imperfections of the crystal and its finite-size. We discuss the role of finite-size effects that inadvertently modify the local density of optical states (LDOS) using time-resolved decay rate measurements from the single domains of real synthesized photonic crystals. We have obtained 34% contrast in the measured emission lifetimes at the stop gap wavelength in comparison to a wavelength outside the stop gap. We have shown a remarkable variation in the emission lifetimes at the stop gap for several domains across the sample which is nullified within a single domain. The results manifest wavelength-dependent linear scaling of lifetimes with the finite-size of the crystal domain. This is a signature of direct dependence of LDOS suppression on the crystal's finite-size which is also found to be in accordance with a recent theoretical model. The precise single-domain measurements result in a robust modification of lifetime in an otherwise weakly classified self-assembled photonic crystal.

DOI: 10.1103/PhysRevA.102.013502

I. INTRODUCTION

The necessity to control the vacuum-fluctuation-induced spontaneous emission nurtured the idea of photonic crystals [1,2]. Based on Fermi's "golden rule," in the weak coupling regime, the spontaneous emission rate can be modified by engineering the density of optical states (DOS) where DOS refers to the number of optical states that are available for the emitted photon at a certain frequency in the medium [3,4]. Photonic crystals are proposed as a platform to modify spontaneous emission which is otherwise considered as an entity that cannot be altered [1–5]. These crystals are constructed with a periodic modulation of dielectric constant on an optical wavelength scale in one (1D), two (2D), or three (3D) spatial dimensions. This periodicity transforms the dispersion relation for light in a particular propagation direction by the opening of a photonic stop gap for certain frequencies that satisfy the Bragg diffraction condition [2,6]. For a 3D photonic crystal, the photonic band gap can be realized if the light propagation, as well as the emission, is prohibited in all spatial directions for any polarization states of light [7,8]. The stringent requirements for the preparation of 3D photonic crystals with photonic band gap have limited its use and therefore, the impact of photonic stop gaps in 3D self-assembled photonic crystals is pursued rigorously [7–12]. The stop gap evokes a direction-dependent inhibition of spontaneous emission for an emitter embedded inside the crystal [13–17]. The stop gap gives rise to local variations in DOS subjected to the position of the emitter and, hence, its relative direction of emission that is represented by the local density of optical states (LDOS) surrounding the emitter.

The theoretical calculations show only a feeble reduction of LDOS with nonzero value at the stop gap due to low-index-contrast of self-assembled photonic crystals with minimal changes in emission intensity and rate [13,18–20]. In synthesized photonic crystals, the LDOS change is further weakened due to the finite-size of the crystal and inherent crystal imperfections, which are circumvented in the theoretical calculations based on the assumption of ideal photonic crystals with an infinite size [18]. The synthesized self-assembled photonic crystal is polycrystalline in nature with micron-sized domains separated by grain boundaries, and it possesses intrinsic defects such as lattice dislocations, stacking faults, and point defects [21,22]. Therefore, the results obtained from the macroscopic emission measurements on the synthesized crystal involving thousands of domains always deviate from the theoretically predicted values. Now, the naive question is when the synthesized photonic crystal can be approximated to be close to an ideal system with minimal disorder. The effect of unintentional disorders can be minimized by performing precise optical measurements from the single domain of the crystal [23,24]. The stop gap measurements from the single domain indicate nearly 100% peak reflectivity unlike the 40%–60% peak reflectivity obtained from the macroscopic measurements [21–24]. This suggests the affinity of a single domain to an ideal crystal with minimal disorder that transpires robust emission suppression at the stop gap [25]. It is seen that the amount of suppression obtained at the stop gap varies across the domains in the sample indicating spatial-dependent fluctuation of LDOS in photonic crystals. This fluctuation arises due to the finite-size of the crystal which may lead to the scaling of LDOS at the stop gap with crystal size. The theoretical modeling and numerical calculations of DOS are done on 2D and 3D band

*Present address: Centre de Nanosciences et de Nanotechnologies (C2N), CNRS, Université Paris-Sud, Université Paris-Saclay, 10 Boulevard Thomas Gobert, 91120 Palaiseau, France.
†rvnair@iitrpr.ac.in

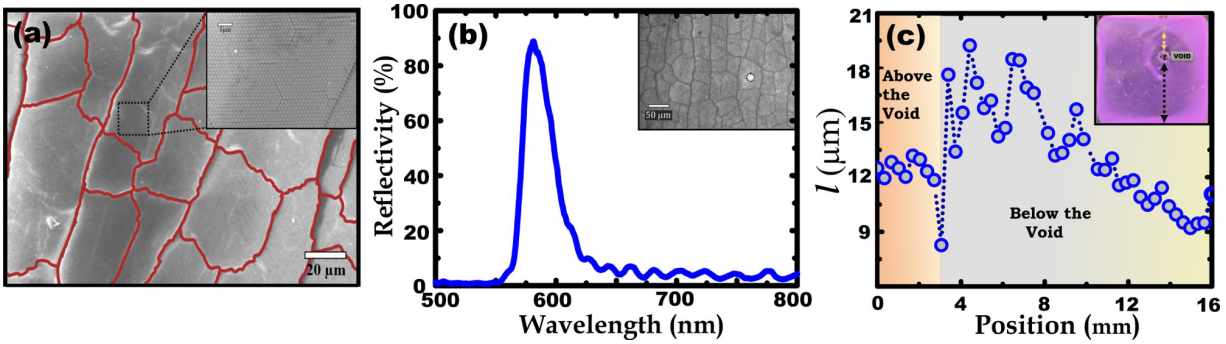

FIG. 1. (a) The SEM image of the sample A highlighting the formation of domains (marked with red lines). The inset shows the zoomed-in SEM image acquired within a domain that shows the hexagonal ordering of the spheres. (b) The measured reflectivity spectra as a function of wavelength precisely obtained from a selected single domain of the crystal with nearly 100% reflectivity at the stop gap. The inset shows the image of the beam focused within a single domain acquired during measurements. (c) The variation of l value across the sample in the measured direction (dotted lines) as depicted in the inset image.

gap crystals that unveil its scaling at the band gap with the crystal's finite-size [26–29]. In experiments, the modification of DOS is evidenced by the change in emission decay rate as inferred from Fermi's "golden rule." The experimental studies on the finite-size-induced modification in emission decay rates are scarcely explored. Therefore, the emission decay rate measurements are required to endorse the finite-size-induced changes in DOS in photonic crystals.

In the present manuscript, we have discussed the finite-size-induced changes in the emission lifetimes using 3D self-assembled photonic crystals as a model system that shows an inherent thickness variation across the sample by virtue of its growth mechanism. We have performed time-resolved decay rate experiments on the single domains of self-assembled photonic crystals. The high-grade photonic effects from a single domain favor strong LDOS changes validated by the sharply modified lifetimes. The finite-size effects are delineated by analyzing the wavelength-dependent emission lifetime values across several domains with different topology and size.

The paper is organized as follows. The sample preparation and the details of experimental setups are discussed in Sec. II. The results obtained are elaborated upon and discussed in Sec. III. The high value of optical reflectivity measured from the single domain of the sample with varying thickness is discussed. The scaling of lifetime values for several domains across the sample is assessed along with the analysis of wavelength-dependent fluctuation in lifetime across and within a single domain of photonic crystal samples. Section IV presents the concluding remarks.

II. SAMPLES AND EXPERIMENTAL DETAILS

The photonic crystal samples are prepared using commercially procured (microParticles, GmbH) polystyrene (PS) microspheres of certain diameter (d) having a refractive index 1.59 doped with rhodamine B (RhB) dye molecules, which acts as the emitter. We have specified the value of $d = 277 \pm 20$ nm to achieve an overlap of the peak emission wavelength of the RhB dye molecule with stop gap at normal incidence. The two samples (A and B) are prepared with the same d on a cleaned glass substrate of dimension 2.5 cm × 2.5 cm using the inward growing self-assembly method [30]. We have also prepared another sample (sample C) with similar d value using a different synthesis method to replicate the results. The sample C is grown on a 1.5 cm × 5.0 cm glass substrate using the convective self-assembly method [22]. Figure 1(a) represents the scanning electron microscope (SEM) image of the sample A which is composed of micron-sized crystal domains of varying size and shape (marked with red lines). The size of the domain at the sample boundary is as large as 200 μm × 200 μm which reduces to as small as 50 μm × 50 μm toward the central region on the sample. The inset of Fig. 1(a) shows the zoomed-in SEM image where long-range hexagonal ordering of PS microspheres within the crystal domain represents the (111) plane of a photonic crystal with face-centered cubic symmetry [21]. The samples B and C also show domains of varying sizes across the sample similar to sample A. We have designed in-house microreflectivity and time-resolved emission experimental setups to measure the stop gap and the subsequent modification of spontaneous emission from the single domain of the photonic crystal. The microreflectivity setup uses a supercontinuum laser source (Fianium) focused using a reflective objective (Edmund Optics) of 0.50 NA (numerical aperture) with 36× magnification that results in spot size of 4 μm in diameter, which is much less than the size of the single domain [31]. The reflected light is collected by the same objective and then fed to a fiber which is connected to a minispectrometer (Avantes).

In the time-resolved emission setup, the sample is excited using a 532-nm pulsed diode laser (52 ps; 10 MHz, PicoQuant, GmbH) focused onto a single domain using a 10× refractive objective of 0.25 NA. The emitted signal is collected from the depth of the sample using the same objective in the confocal geometry and sent to a single-photon avalanche diode (SPAD) detector (PicoQuant, GmbH). The emission at the required wavelength is selected using 570 ± 10 nm and 600 ± 10 nm narrow-bandpass filters. The excitation laser and SPAD detector are synchronized with a time-correlated single-photon counting unit (HydraHarp 400, PicoQuant, GmbH), which records the time difference between the excitation and emission (arrival) events. The instrument response function (IRF) for the setup is measured to be ∼0.08 ns which determines the overall timing resolution of the measurements. The IRF value is much less than the typical lifetime (∼2 ns) of

RhB dye and, therefore, the lifetime can be estimated without the deconvolution of the IRF from the measured decay curve. Both experimental setups are equipped with an *in situ* optical microscope that helps in positioning the incident laser beam on a single domain using an *x-y-z* translation stage with a resolution of 50 nm (Physik Instrumente, GmbH).

III. RESULTS AND DISCUSSION

A. Single-domain reflectivity measurements

Figure 1(b) shows the reflectivity spectrum precisely measured from the center region of a selected single domain (see inset) of sample A. The photonic stop gap in the [111] direction is centered at 585 nm with a peak reflectivity of 90%. The measured stop gap wavelength (λ_g) is slightly less than the calculated value of 600 nm using the Bragg diffraction condition at normal incidence [32]. The calculation of λ_g is done for an interplanar spacing (d_{111}) of 209 nm and an effective refractive index of 1.44. The blueshift in the measured value of λ_g is attributed to the angle averaging in the reflectivity measurements due to the high NA of the objective. It is observed that each domain possesses a unique orientation which can also cause a shift in the measured λ_g. Therefore, we have obtained an average value of λ_g as 586 $\pm$ 2 nm with a variation in the peak reflectivity values from 7% to 94% across the sample over 50 domains. Evidently, for domains with discrete orientations across the sample, the λ_g value remains nearly the same which supports the fine structural quality of the domains [21,33]. The unintentional disorders are minimized within a domain and, therefore, the single domain is a good approximation to an ideal crystal with minimal disorders.

The single-domain microreflectivity measurements yield a sharp and intense Fabry-Perot fringe pattern in the long-wavelength limit as seen in Fig. 1(b), which helps in the estimation of thickness (l) of a particular domain [32]. The estimated l value for the selected single domain shown in Fig. 1(b) is 8.1 $\pm$ 0.4 μm. Figure 1(c) unfolds the variation of the l value across the sample induced by the growth inception [21]. The microreflectivity measurements are performed along the direction marked on the photographic image [inset of Fig. 1(c)] of sample A. The image shows a void space created due to the lack of microspheres to form the crystal layers at the end of the growth process [30]. The single domains are picked along a line (16 mm long; black dotted line) at an interval of 0.34 mm to avoid the overlap between the successive reflectivity measurements. This scan reveals domains with a high l value close to the void which is then gradually reduced toward the sample boundary. The l value varies from 8 to 20 μm for different domains across the sample which corresponds to 38–95 layers and thus the finite-size effects are avoided in reflectivity measurements [21]. The l value also tends to reduce for the domains above the void (yellow dotted line) as seen in Fig. 1(c).

The strength of light-matter interaction in a photonic crystal is discussed through a parameter called the photonic interaction strength (S) [34]. The S parameter determines the coupling strength of the incident light with a photonic crystal which is related to the polarizability of the scatterers

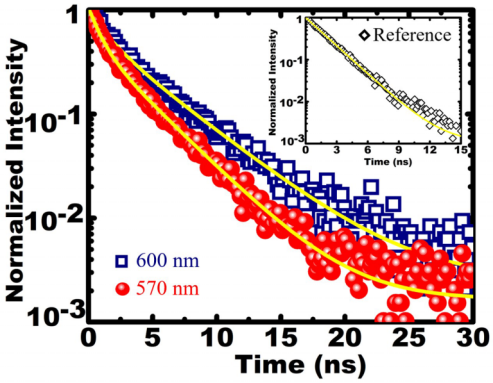

FIG. 2. The measured emission decay curves at 570 nm (red spheres) and 600 nm (blue squares) for sample A. The inset shows the decay curve for the reference sample (black diamonds). Solid lines are the suitable exponential fits to the measured decay curves.

(PS microspheres) in the sample. The S value is strongly influenced by the dielectric contrast and the finite-size of the crystal and its value is obtained by taking the ratio of the measured reflectivity peak linewidth ($\Delta\lambda$) to λ_g. The S parameter is related to the characteristic attenuation length for light propagating inside the crystal at the stop gap known as the Bragg length (L_B) which is estimated as $L_B = \frac{2d_{111}}{\pi S}$ [33]. Thus the value of S and hence the L_B determines the strength of light-matter interaction in photonic crystals. The average value of S and L_B obtained from the measurements over 50 single domains are 5.6 $\pm$ 0.3% and 2.6 $\pm$ 0.1 μm, respectively. The comprehensive modulation of l and L_B values across the domains accounts for the prominent role of finite-size effects which have consequences in the modification of emission decay rates as discussed in the following.

B. Single-domain decay rate measurements

The single-domain decay rate measurements are conducted at a wavelength of 600 nm which corresponds to the stop gap and at a wavelength of 570 nm which is outside the stop gap. The two wavelengths are specifically chosen to obtain wavelength-dependent change in the decay rates and thus the redistribution of LDOS in a self-assembled photonic crystal. The measured decay rates for the photonic crystal sample are also compared with a reference sample, which is a colloidal suspension of RhB dye–doped PS spheres that provides wavelength-independent decay rates. Figure 2 displays the measured emission decay curves at 570 nm (red spheres) and 600 nm (blue squares) for sample A. The measured decay curve is slower at 600 nm in comparison to the decay curve at 570 nm. The inset of Fig. 2 shows the measured decay curve at 600 nm for the reference sample (black diamonds) which shows a much faster decay in comparison to sample A. The slower decay measured at 570 nm for sample A in comparison to the reference sample is caused by the change in effective refractive index of the medium [35,36]. The decay curve is slowed down at 600 nm for sample A which is due to the LDOS suppression within the photonic stop gap. The difference in the decay curves at 570 and 600 nm for sample A recommends the finite reduction of LDOS at the stop gap

in photonic crystals that results in a wavelength-dependent lifetime distribution.

The decay curve for the reference sample is fitted (solid line) with a single exponential decay function as seen in Fig. 2 (inset). The estimated lifetime for the reference sample is 1.9 ns, in agreement with the reported lifetime value for the RhB dye suspension [36,37]. The measured decay curves for sample A (at 570 and 600 nm) are best fitted (solid line) with a double exponential decay function comprising shorter and longer lifetime components due to the presence of an inhomogeneous environment around the emitter [35]. The measured decay curves for sample A are fitted using the equation $I(t) = n_1 \exp(-\frac{t}{\tau_1}) + n_2 \exp(-\frac{t}{\tau_2})$ where $I(t)$ is the emission intensity decaying with time t; n_1 and n_2 are the amplitudes corresponding to the lifetime components τ_1 and τ_2 that are associated with slower or faster decay processes, respectively. We have obtained an effective lifetime value as $\langle\tau\rangle = \frac{n_1\tau_1}{n_1\tau_1+n_2\tau_2}\tau_1 + \frac{n_2\tau_2}{n_1\tau_1+n_2\tau_2}\tau_2$ [13]. The τ_1 and τ_2 values are around 4–5 ns and 1 ns, respectively, for sample A. It is proposed that, for the RhB dye molecules attached to the PS spheres, the longer decay component is attributed to the influence of the PS lattice framework, while the shorter component is assigned to a rapid nonradiative decay process such as the strong interaction between nearby dye molecules [36]. The estimated $\langle\tau\rangle$ value at 570 and 600 nm is 2.9 and 3.9 ns, respectively. The 51% increase in the $\langle\tau\rangle$ value at 600 nm for sample A in comparison to the reference sample evinces a stronger LDOS suppression at the stop gap. Also, there is a 34% increase in the $\langle\tau\rangle$ value at λ_g (600 nm) in comparison to the $\langle\tau\rangle$ value for a wavelength outside the stop gap (570 nm) for sample A. This indicates a 2.5× inhibition of spontaneous emission at λ_g using the single domain of the sample. This variation in $\langle\tau\rangle$ value is at par with an emission modification for emitters embedded in inverse opals offering high dielectric contrast, which reports a 30% enhancement of the lifetime at the stop gap [38]. This further supports the applicability of a single domain in obtaining the strong photonic effects in the otherwise weakly classified low-index-contrast self-assembled photonic crystals.

We observe a strong variation in $\langle\tau\rangle$ values at λ_g for different domains across the sample which is caused by the difference in the finite-size of domains across the sample. This will serve as evidence of the finite-size-induced spatial fluctuation in LDOS in synthesized photonic crystal samples. The finite-size effects are explicated using the l and L_B values obtained from the single-domain reflectivity scan on sample A in the same direction as that of the decay rate measurements. The value of L_B alone cannot be used to scale the finite-size effects as L_B gauges the light-matter interaction in the few layers of the sample depth. In the same way, the value of l often endures the intrinsic disorder and defects present in the depth of the crystal. Hence the ratio l/L_B is used to properly account for both the finite-size of the domain and any effect induced by the inherent disorder within a particular domain. Therefore, the quantity l/L_B is used to scale the variation of $\langle\tau\rangle$ values across the sample.

Figures 3(a) and 3(b) show the variation of $\langle\tau\rangle$ value at 600 nm (blue squares) and 570 nm (red spheres) as a function of l/L_B, respectively. A linear variation in the $\langle\tau\rangle$ value is obtained at 600 nm with a variation from 3.4 to 3.8 ns for an increase in l/L_B value from 3.8 to 6.3. The increase in the $\langle\tau\rangle$ value at the stop gap with l/L_B implies enhanced LDOS suppression at higher values of l/L_B. An overall increase of 0.4 ns is measured for $\langle\tau\rangle$ values at 600 nm with l/L_B for sample A. In contrast, the $\langle\tau\rangle$ values at 570 nm do not scale with l/L_B as seen in Fig. 3(b). The $\langle\tau\rangle$ values at 570 nm are scattered around an average $\langle\tau\rangle$ value of 3.1 ± 0.1 ns. This shows that the measured $\langle\tau\rangle$ values for a wavelength outside the stop gap are independent of the finite-size of the domains. The appreciable linear scaling of $\langle\tau\rangle$ values at 600 nm with l/L_B is obtained due to the high photonic quality of single domains even though the samples exhibit low-index-contrast.

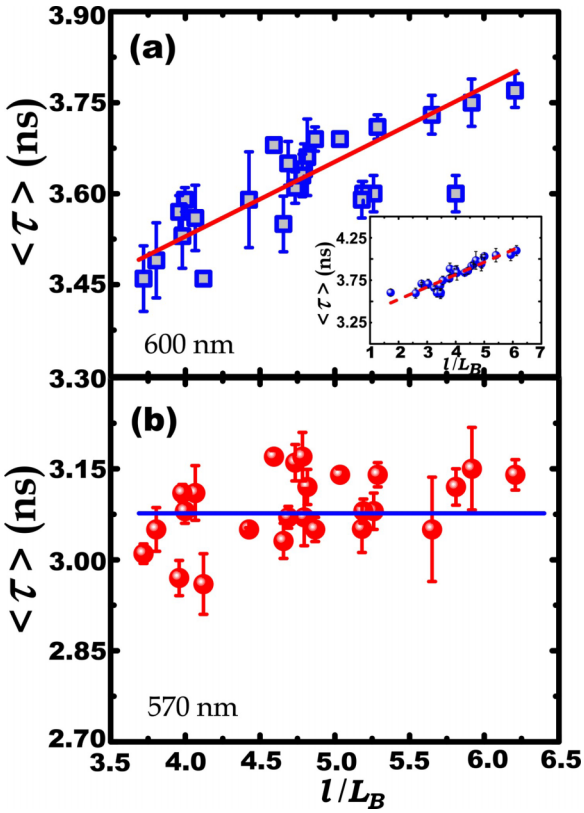

FIG. 3. The variation of $\langle\tau\rangle$ values at (a) 600 nm (blue squares) and (b) 570 nm (red spheres) across the sample A as a function of l/L_B. The solids line in (a,b) show a linear fit to the measured data. The inset shows a linear variation of $\langle\tau\rangle$ values with l/L_B at 600 nm for sample C along with a linear fit (dashed line).

We have also investigated the effect of topology and physical dimensions of the sample on the scaling of $\langle\tau\rangle$ values at 600 nm using sample C. Sample C shows a radical formation of domains of varying topology in the growth direction [21]. The domains possess large dimensions and high l value at the growth inception that reduces to the end of the sample area due to the scarcity of the PS microspheres in the suspension. The average λ_g value for sample C obtained from the microreflectivity measurements on several single domains is 584 ± 4 nm with a variation in l values from 3 to 15 μm. The peak reflectivity values for different domains also vary from 35% to nearly 100% across the sample. The inset of Fig. 3(a) disseminates the variation in $\langle\tau\rangle$ values from 3.6 to 4.1 ns at 600 nm with a change in l/L_B from 1.7 to 6.1. Evidently, the

$\langle\tau\rangle$ values for sample C also show a linear scaling with l/L_B with an overall variation of 0.5 ns similar to sample A.

C. Spatial variation in the emission lifetimes

In order to quantify the fluctuation in the $\langle\tau\rangle$ values across the sample, we have done a detailed scan on sample B by measuring the emission decay curves for more than 250 single domains. Sample B is preferred to replicate $\langle\tau\rangle$ value fluctuation on another sample prepared under the same growth conditions as sample A. The observed variation of $\langle\tau\rangle$ values at 600 nm along the measured direction on sample A incited us to perform measurements from the other different areas of the sample. Thus wavelength-dependent $\langle\tau\rangle$ values are acquired using the decay rate measurements from the single domains in a spider-web-like scan geometry on sample B as illustrated in the inset of Fig. 4(a). The scanning scheme is divided into five squares that identify the areas having domains with different l values and dimensions. The two consecutive squares are 2.5 mm apart from each side. Starting with square 1 (dashed line) that is nearly equal to the dimensions of the substrate allows us to probe the domains near the sample boundary. The size of the square begins to reduce as the scan moves toward square 5 (solid line) in the middle of the sample. The single domains are selected along each side of the square with a separation of 1 mm between the two successive domains. The $\langle\tau\rangle$ values are acquired for every single domain picked on each side of all five squares. The measurements are acquired from 100 domains in square 1 which is reduced in steps of 20 to the innermost square 5. The $\langle\tau\rangle$ values are extracted from the fit to the measured decay curves at 570 and 600 nm for all the domains in each of the squares.

Figure 4(a) shows the variation of mean $\langle\tau\rangle$ value (which is averaged over many domains in each of the squares) as a function of the square number. The mean $\langle\tau\rangle$ value at 570 and 600 nm is evaluated for each square scan on sample B. The mean $\langle\tau\rangle$ values are fitted with a linear function (dashed line) that depicts a higher slope and hence larger variation at 600 nm in comparison to the slight variation at 570 nm. The minimal scaling observed for mean $\langle\tau\rangle$ values at 570 nm is due to the partial overlap of the short-wavelength stop gap edge of sample B. It is observed that the mean $\langle\tau\rangle$ value decreases linearly toward square 5 or toward the middle of the sample for both 570 and 600 nm. The mean $\langle\tau\rangle$ values at 570 nm and 600 nm overlap each other for square 5 which shows similar LDOS values at both wavelengths. This infers that there are certain domains in the square 5 region where similar $\langle\tau\rangle$ values are obtained at 570 and 600 nm and become comparable to the reference lifetime of RhB dye doped in the bulk PS medium [39]. The highest difference between the $\langle\tau\rangle$ values at 570 and 600 nm for a selected single domain in the square 1 scan is obtained as 0.85 ns, suggesting a maximum LDOS suppression. The notable wavelength-dependent change in the $\langle\tau\rangle$ value is within the limit of 1 ns as predicted for an ideal self-assembled photonic crystal with an S value of 6.5% [39].

As discussed, the vivid distribution of $\langle\tau\rangle$ values at 600 nm is a direct consequence of the role of finite-size-induced modification of LDOS in a photonic crystal. The role of unintentional disorder and defects is minimized in the decay rate measurements as it is obtained from the single domains of the crystal. Thus, to further prove the merits of using the single domain for emission measurements, the decay curves are also measured at 570 and 600 nm from the several spatial positions within a selected domain. Figures 4(b) and 4(c) depict the histogram of the estimated $\langle\tau\rangle$ values at 570 nm (red bars) and 600 nm (blue bars) from the decay rate measurements on several single domains and also within a particular domain picked from the square 1 region of sample B. The histogram distribution is best fitted by a Gaussian function to extract the mean of the $\langle\tau\rangle$ values and the distribution width

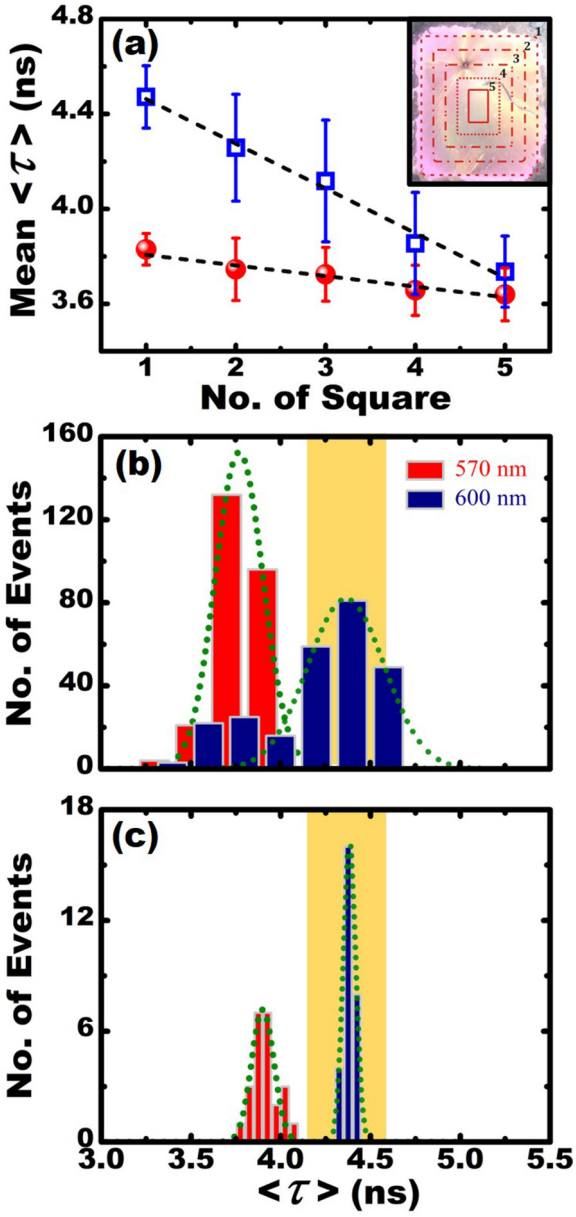

FIG. 4. (a) The variation of mean $\langle\tau\rangle$ values at 570 (spheres) and 600 nm (squares) as a function of the square number involved in the spider-web-like scan on the sample B (inset). The histograms of the $\langle\tau\rangle$ values at 570 (red bars) and 600 nm (blue bars) fitted with a Gaussian distribution function (dotted line) that shows different distribution width (b) across the domains and (c) within a single domain.

(w). The mean of the $\langle\tau\rangle$ value distribution is 3.8 ns with $w = 0.26$ ns and 4.4 ns with $w = 0.43$ ns at 570 and 600 nm, respectively. The value of w is doubled for 600 nm in comparison to the same at 570 nm, which shows that the $\langle\tau\rangle$ values at 600 nm are more sensitive to the changes in the LDOS caused by the finite-size effects as seen in Fig. 4(b). The histogram distribution of $\langle\tau\rangle$ values within a single domain at 570 and 600 nm is shown in Fig. 4(c). The mean of the $\langle\tau\rangle$ value distribution obtained using the fit is 3.9 ns with $w = 0.12$ ns and 4.4 ns with $w = 0.07$ ns for 570 nm and 600 nm, respectively. The w value shows an 84% decrease within a single domain in comparison to the w value obtained across the sample at 600 nm, which accounts for the minimum LDOS fluctuation within a single domain. Therefore, the large w value obtained from the $\langle\tau\rangle$ value distribution at 600 nm across the domains is an outcome of LDOS fluctuations.

The observed spatial fluctuation in the $\langle\tau\rangle$ value across the domains corroborates the role of finite-size effect in the LDOS suppression in synthesized photonic crystal samples. The $\langle\tau\rangle$ value fluctuation at 600 nm is very much narrowed within a single domain in relation to the same across the sample. In contrast, the $\langle\tau\rangle$ values at 570 nm show trivial fluctuation in LDOS across the sample as well as within a domain. This is due to the stronger LDOS changes at 600 nm in comparison to the LDOS change at 570 nm. The distinctive variation of the emission lifetimes at 570 and 600 nm corroborates the wavelength-dependent characteristics of LDOS around the stop gap. The measured wavelength-dependent changes in the emission lifetime evince 34% longer lifetimes for an emitter emitting at the stop gap wavelength. Certainly, the results have aided in discerning the strong inhibition of LDOS in the low-index-contrast self-assembled photonic crystals using the precise single-domain measurements. The spatial variation of the $\langle\tau\rangle$ value pinpoints stronger LDOS dependence on the finite-size of the crystal domain which is parametrized by l/L_B.

We have demonstrated the extent of change in the emitter lifetime that can be observed in a finite-sized self-assembled photonic crystal. The results ratify the linear increase in lifetime values at the stop gap with an increase in the finite-size of the crystal domains. The linear variation of lifetime shows a close resemblance to the DOS scaling in a 3D photonic band gap crystal [29]. Consequently, the emission decay rates can be modulated not only on the basis of frequency and position but also using the finite-size of synthesized photonic crystals as a result of the reconstruction of LDOS at the stop gap. The light-matter interaction can be tailored precisely with significant engineering in the light transport and emission measurements performed on the structured environment. This allows us to exploit the scalable architecture created by photonic devices to utilize in wide applications of quantum information processing which requires an efficient quantum interface between light and matter. The photonic crystal structures form a basis for solid-state quantum photonics integrated with a single quantum emitter for the efficient nonclassical light generation and improve the performance of single-photon devices.

IV. CONCLUSIONS

Single-domain spectroscopy plays a significant role in revealing the enigmatic optical response of the photonic crystal in parallel to the theoretical predictions. The reflectivity spectra from different domains exhibit the impressions of finite-size effects that lead to the prevailing fluctuation in emission lifetime at the stop gap. We have studied the finite increase in the lifetime values due to the reduction in LDOS at the stop gap for an embedded emitter in self-assembled photonic crystals. Remarkably, we have observed a significant wavelength-dependent modification of lifetime values with an overall 34% increase in the emission lifetime at the stop gap with respect to the wavelength outside the stop gap. The emission lifetime measurements exhibit sizable variation of lifetime values at the stop gap across several domains that validate a spatially dependent LDOS variation in synthesized photonic crystal. The LDOS fluctuation is originated due to the difference in the finite-size of the crystal domain across the sample. The lifetime values at the stop gap show a linear scaling with l/L_B which substantiates a linear variation in the LDOS suppression. Our results establish the fact that LDOS is inversely proportional to the finite-size of the real photonic crystal. The observed scaling of LDOS in a 3D photonic crystal displays a qualitative agreement with theoretically predicted linear variations of DOS with the crystal size. The study acclaims precise control on the spontaneous emission with respect to the finite-size of the crystal that will aid in the construction of devices based on photonic crystals.

ACKNOWLEDGMENTS

The authors would like to acknowledge the financial support from IIT Ropar (ISIRD Grant, 2014), DST-SERB (FTS/PS-80/2014), and CSIR [03(1352)/16/EMR-II]; Government of India. The authors would like to thank Sachin Sharma for help in setting up the time-resolved experiment. We acknowledge IIT Ropar for the use of the scanning electron microscope. M.K. and Priya thank IIT Ropar for financial support through the Ph.D. fellowship and Honourable Director's fellowship, respectively.

M.K. and Priya contributed equally to this work.

[1] V. P. Bykov, Spontaneous emission in a periodic structure, Sov. Phys. JETP **35**, 269 (1972); Spontaneous emission from a medium with a band structure, Sov. J. Quantum Electron. **4**, 861 (1975).

[2] E. Yablonovitch, Inhibited Spontaneous Emission in Solid State Physics and Electronics, Phys. Rev. Lett. **58**, 2059 (1987).

[3] R. Loudon, *The Quantum Theory of Light* (Clarendon Press, Oxford, 1983).

[4] W. L. Barnes, S. A. R. Horsley, and W. L. Vos, Classical antennas, quantum emitters, and densities of optical states, J. Opt. **22**, 073501 (2020).

[5] M. Pelton, Modified spontaneous emission in nanophotonic structures, Nat. Photonics **9**, 427 (2015).

[6] C. Lopez, Material aspects of photonic crystals, Adv. Mater. **15**, 1679 (2003).

[7] S. R. Huisman, R. V. Nair, L. A. Woldering, M. D. Leistikow, A. P. Mosk, and W. L. Vos, Signature of a three-dimensional photonic band gap observed with silicon inverse woodpile photonic crystals, Phys. Rev. B **83**, 205313 (2011).

[8] M. D. Leistikow, A. P. Mosk, E. Yeganegi, S. R. Huisman, A. Lagendijk, and W. L. Vos, Inhibited Spontaneous Emission of Quantum Dots Observed in a 3D Photonic Band Gap, Phys. Rev. Lett. **107**, 193903 (2011).

[9] M. R. Jorgensen, J. W. Galusha, and M. H. Bartl, Strongly Modified Spontaneous Emission Rates in Diamond-Structured Photonic Crystals, Phys. Rev. Lett. **107**, 143902 (2011).

[10] W. L. Vos, A. F. Koenderink, and I. S. Nikolaev, Orientation-dependent spontaneous emission rates of a two-level quantum emitter in any nanophotonic environment, Phys. Rev. A **80**, 053802 (2009).

[11] D. Devashish, O. S. Ojambati, S. B. Hasan, J. J. W. van der Vegt, and W. L. Vos, Three-dimensional photonic band gap cavity with finite support: Enhanced energy density and optical absorption, Phys. Rev. B **99**, 075112 (2019).

[12] S. Sharma and R. V. Nair, Nanophotonic control of the color center emission from nanodiamonds, Opt. Lett. **43**, 3989 (2018).

[13] M. Barth, A. Gruber, and F. Cichos, Spectral and angular redistribution of photoluminescence near a photonic stop band, Phys. Rev. B **72**, 085129 (2005).

[14] M. Li, P. Zhang, J. Li, J. Zhou, A. Sinitskii, V. Abramova, S. O. Klimonsky, and Y. D. Tretyakov, Directional emission from rare earth ions in inverse photonic crystals, Appl. Phys. B **89**, 251 (2007).

[15] B. H. Husken, A. F. Koenderink, and W. L. Vos, Angular redistribution of near-infrared emission from quantum dots in three-dimensional photonic crystals, J. Phys. Chem. C **117**, 3431 (2013).

[16] R. V. Nair, A. K. Tiwari, S. Mujumdar, and B. N. Jagatap, Photonic-band-edge-induced lasing in self-assembled dye-activated photonic crystals, Phys. Rev. A **85**, 023844 (2012).

[17] S. Wu, H. Xia, J. Xu, X. Sun, and X. Liu, Manipulating luminescence of light emitters by photonic crystals, Adv. Mater. **30**, 1803362 (2018).

[18] J. Gutmann, H. Zappe, and J. C. Goldschmidt, Quantitative modeling of fluorescent emission in photonic crystals, Phys. Rev. B **88**, 205118 (2013).

[19] A. F. Koenderink, L. Bechger, H. P. Schriemer, A. Lagendijk, and W. L. Vos, Broadband Fivefold Reduction of Vacuum Fluctuations Probed by Dyes in Photonic Crystals, Phys. Rev. Lett. **88**, 143903 (2002).

[20] E. Pavarini, L. C. Andreani, C. Soci, M. Galli, F. Marabelli, and D. Comoretto, Band structure and optical properties of opal photonic crystals, Phys. Rev. B **72**, 045102 (2005).

[21] J. F. Galisteo-Lopez, E. Palacios-Lidon, E. Castillo-Martinez, and C. Lopez, Optical study of the pseudogap in thickness and orientation controlled artificial opals, Phys. Rev. B **68**, 115109 (2003).

[22] J. F. Galisteo-López, M. Ibisate, R. Sapienza, L. S. Froufe-Pérez, Á. Blanco, and C. López, Self-assembled photonic structures, Adv. Mater. **23**, 30 (2011).

[23] Y. A. Vlasov, M. Deutsch, and D. J. Norris, Single-domain spectroscopy of self-assembled photonic crystals, Appl. Phys. Lett. **76**, 1627 (2000).

[24] J. F. Galisteo Lopez and W. L. Vos, Angle-resolved reflectivity of single-domain photonic crystals: Effects of disorder, Phys. Rev. E **66**, 036616 (2002).

[25] Priya and R. V. Nair, Scaling the spatial fluctuation of spontaneous emission suppression in photonic crystals, Opt. Lett. **44**, 2811 (2019).

[26] D. M. Whittaker, Inhibited emission in photonic woodpile lattices, Opt. Lett. **25**, 779 (2000).

[27] K. Ishizaki, M. Okano, and S. Noda, Numerical investigation of emission in finite-sized, three-dimensional photonic crystals with structural fluctuations, J. Opt. Soc. Am. B **26**, 1157 (2009).

[28] E. Yeganegi, A. Lagendijk, A. P. Mosk, and W. L. Vos, Local density of optical states in the band gap of a finite one-dimensional photonic crystal, Phys. Rev. B **89**, 045123 (2014).

[29] S. B. Hasan, A. P. Mosk, W. L. Vos, and A. Lagendijk, Finite-Size Scaling of the Density of States in Photonic Band Gap Crystals, Phys. Rev. Lett. **120**, 237402 (2018).

[30] R. V. Nair and R. Vijaya, Structural and optical characterization of photonic crystals synthesized using the inward growing self-assembling method, Appl. Phys. A **90**, 559 (2008).

[31] S. Sharma, Priya, S. Saini, and R. V. Nair, A versatile micro-reflectivity set-up for probing the optical properties of photonic nanostructures, Rev. Sci. Instrum. **90**, 023103 (2019).

[32] Priya and R. V. Nair, Polarization-selective branching of stop gaps in three-dimensional photonic crystals, Phys. Rev. A **93**, 063850 (2016).

[33] R. V. Nair and B. N. Jagatap, Bragg wave coupling in self-assembled opal photonic crystals, Phys. Rev. A **85**, 013829 (2012).

[34] W. L. Vos, A. Lagendijk, and A. P. Mosk, *Light Localisation and Lasing: Random and Pseudorandom Photonic Structures*, edited byM. Ghulinyan and L. Pavesi (Cambridge University Press, Cambridge, UK, 2015), Chap. 1.

[35] Priya, O. Schöps, U. Woggon, and R. V. Nair, Inhibited spontaneous emission using gaplike resonance in disordered photonic structures, Phys. Rev. A **98**, 043835 (2018).

[36] G. Scalia and F. Scheffold, Lifetime of fluorescent dye molecules in dense aqueous suspensions of polystyrene nanoparticles, Opt. Express **23**, 29342 (2015).

[37] N. Boens, W. Qin, N. Basarić, J. Hofkens, M. Ameloot, J. Pouget, J.-P. Lefèvre, B. Valeur, E. Gratton, M. van deVen *et al.*, Fluorescence lifetime standards for time and frequency domain fluorescence spectroscopy, Anal. Chem. **79**, 2137 (2007).

[38] P. Lodahl, A. F. Van Driel, I. S. Nikolaev, A. Irman, K. Overgaag, D. Vanmaekelbergh, and W. L. Vos, Controlling the dynamics of spontaneous emission from quantum dots by photonic crystals, Nature **430**, 654 (2004).

[39] M. Megens, J. E. G. J. Wijnhoven, A. Lagendijk, and W. L. Vos, Fluorescence lifetimes and linewidths of dye in photonic crystals, Phys. Rev. A. **59**, 4727 (1999).